processes

MDPI

Article

Sodium Alginate–Soy Protein Isolate–Chitosan–Capsaicin–Nanosilver Multifunctional Antibacterial Composite Gel

Zhichao Zhang [1,†], Meizi Huang [2,3,†], Kejian Shen [4,†], Yucai He [4,*] and Youyan Liu [1,*]

[1] School of Chemistry and Chemical Engineering, Guangxi University, Nanning 530004, China; zhangzhichao9088@163.com
[2] Jiangsu ShenQi Medicine Technology Co., Ltd., Danyang 212353, China; huang201833@163.com
[3] School of Animal Pharmacy, Jiangsu Agri-Animal Husbandry Vocational College, Taizhou 225300, China
[4] School of Pharmacy & School of Biological and Food Engineering, Changzhou University, Changzhou 213164, China; shenkejiancczu@163.com
* Correspondence: heyucai2001@163.com (Y.H.); liuyouyangx@163.com (Y.L.)
† These authors contributed equally to this work.

Abstract: We constructed a sodium alginate/soy protein isolate/chitosan gel system and incorporated silver nanoparticles reduced by capsaicin into the system, forming a sodium alginate–soy protein isolate–chitosan–capsaicin–silver nanoparticle composite gel (SA/SPI/CTS/CAP/Ag). In tests, the SA/SPI/CTS/CAP/Ag gel exhibited excellent antimicrobial properties. Using the agar diffusion method, the inhibition zone diameter for *Staphylococcus aureus* was determined to be 29.5 mm. Soy protein isolate (SPI), containing a large number of hydrophobic amino acid residues, effectively enhanced the moisture retention capability of the gel and improved its stability to a certain extent at an appropriate addition concentration. In a milk preservation experiment, the SA/SPI/CTS/CAP/Ag gel significantly extended the shelf-life of the milk. In dye adsorption experiments, the adsorption curve of the SA/SPI/CTS/CAP/Ag gel well fitted a pseudo-second-order kinetic model. It showed a degree of adsorption capacity for methylene blue, malachite green, methyl orange, and Congo red, with the most significant adsorption effect for malachite green being 42.48 mg/g. Considering its outstanding antimicrobial performance, preservation ability, and adsorption capacity, the SA/SPI/CTS/CAP/Ag gel holds significant potential in wastewater treatment and as an antimicrobial gel in the exploration of food preservation.

Keywords: antibacterial ability; dye adsorption; milk preservation; nanosilver antibacterial composite; microbial pollution

Citation: Zhang, Z.; Huang, M.; Shen, K.; He, Y.; Liu, Y. Sodium Alginate–Soy Protein Isolate–Chitosan–Capsaicin–Nanosilver Multifunctional Antibacterial Composite Gel. *Processes* **2024**, *12*, 662. https://doi.org/10.3390/pr12040662

Academic Editor: Antoni Sanchez

Received: 4 March 2024
Revised: 20 March 2024
Accepted: 22 March 2024
Published: 26 March 2024

1. Introduction

In recent years, with the rapid advancement of modern industrial technology and the increasing complexity of human lifestyles, water resource pollution has become a growing concern [1,2]. The proliferation of pollutant sources has resulted in the extensive release of contaminants, such as bacteria, heavy metal ions, and dyes, significantly impacting water quality [3]. Dyes are considered highly hazardous pollutants due to their acute toxicity, persistence, and non-biodegradability. The colored components in industrial wastewater are toxic, and their removal remains a complex process. For instance, Congo red dye is an anionic water-soluble dye, particularly used in the leather, textile, biomedical, and cosmetics industries. Dye pollution prevents sunlight from penetrating water bodies, thereby delaying the photosynthesis process of aquatic life [4,5]. To address this series of issues, researchers have turned their focus to the development of antibacterial materials. These materials, with their ability to inhibit the growth and

reproduction of bacteria, find application in water treatment [6,7]. However, antibacterial materials exhibit weak adsorption effects on dyes, and the simultaneous application of antibacterial materials and adsorbents increases the cost in water ponds. Therefore, the preparation of multifunctional adsorption–antibacterial gel composites has sparked broad interest among researchers. Consequently, there is an urgent need to develop an adsorption–antibacterial gel material with multifunctionality, demonstrating excellent antibacterial and adsorption performances. The distinctive properties of silver nanoparticles (AgNPs), along with their various applications at the nanoscale, have aroused widespread interest in the field of antibacterial materials [8]. AgNPs have been extensively utilized in the medical field owing to their strong antibacterial efficacy and minimal damage to the human body [9]. Once AgNPs penetrate the cell membrane, they interact with the alternating negative and positive charges around the membrane, which leads to membrane damage and the leakage of cellular contents, culminating in the deactivation of the bacteria [10]. Capsaicin, the active component found in chili peppers, possesses a variety of biological activities, including antibacterial, antioxidant, anti-tumoral, and analgesic properties [11]. The applications of capsaicin are incredibly diverse; not only is it a significant food additive, but it also plays a unique role in medicine, industry, and other sectors [12,13]. To enhance the stability and bioavailability of capsaicin, a variety of encapsulation technologies have been developed, such as coacervation, emulsification, spray cooling, and liposome delivery [14]. These methods have expanded the use of capsaicin in the food sector. Sodium alginate (SA), chitosan (CTS), and soy protein isolate (SPI) are all natural organic polymers that have extensive applications in fields such as food preservation, wastewater treatment, and antibacterial materials [15–17]. Chitosan, in particular, with its exceptional antibacterial properties, excellent biocompatibility, and adsorption capacity, has been widely applied in medical wound dressings, food safety, and wastewater treatment sectors [18,19]. In recent years, researchers have deeply explored and studied the adsorption performance of chitosan composite materials for dyes [20]. Furthermore, the mechanism of microbial inhibition by chitosan composite materials has increasingly attracted scholarly attention. Therefore, researchers have based their studies on chitosan gel systems, introducing natural organic polymers to alter their physical structures, allowing them to adapt to various wastewater environments [21]. It has been found that chitosan and sodium alginate are often considered cationic and anionic polysaccharides due to their capacity for easy protonation, where part of the carboxyl and amino groups can also be protonated [22]. Hence, these oppositely charged polysaccharide molecules can form polyelectrolyte complexes through electrostatic interactions. Some studies suggest that such polyelectrolyte complexes may amalgamate the properties of sodium alginate and chitosan, exhibiting good biocompatibility and biodegradability [23]. The sodium alginate-chitosan polyelectrolyte complexes are thus considered preferred adsorbents [24]. Soy protein isolate contains many charged and hydrophobic amino acid residues [25,26]. Therefore, leveraging soy protein isolate to enhance the physical properties of gels has captured widespread interest among researchers.

In this work, SA/SPI/CTS/CAP/Ag gel was prepared with SA-CTS polyelectrolyte complex as a carrier, SPI as a polyelectrolyte complex enhancer, and capsaicin-reduced silver nanoparticles as the primary antibacterial substance. The reduced silver nanoparticles were embedded into the gel to minimize the natural loss of nanoparticles, thus enabling the reusability of the gel. The antibacterial properties and synergistic antibacterial mechanisms of the gel material were investigated. The dye adsorption process of the gel was simulated using pseudo-first-order and pseudo-second-order kinetic equations. Based on this, the stability, antibacterial activity, diurnal stability, and preservation effect of the gel were tested. The swelling, dehydration, water absorption, and degradation properties of the gel were evaluated. By establishing kinetic models, the maximum dye adsorption capacity of the material was assessed. The SA/SPI/CTS/CAP/Ag gel composite material exhibits good antibacterial capability. It also possesses exceptional

adsorption capacity, presenting potential applications in water treatment and food preservation.

2. Materials and Methods

2.1. Materials

All reagents used in this study were of analytical grade. $AgNO_3$ (≥99.8%), chitosan (CTS) (molecular weight 1526), sodium alginate (SA) (molecular weight 10,000–60,000), soy protein isolate (SPI) (molecular weight 194), and boric acid (≥99%) were bought from Shanghai Lingfeng Chemicals Co., (Shanghai, China). The chili peppers were obtained from Xiaomiao Road market in Changzhou, China.

2.2. Pretreatment of Chili Peppers

Chili peppers were rinsed multiple times with water to remove surface dust particles. Furthermore, they were dried in a constant temperature oven at 50 °C for 24 h to eliminate all residual moisture. The dried chili peppers were then pulverized using a grinder, and the resulting powder was sieved through an 80-mesh screen for subsequent use. A quantity of 2.5 g of the chili pepper powder was soaked in 50 mL of 95% ethanol and subjected to ultrasonication at a water bath temperature of 80 °C for 30 min [27]. The solution was further filtered using a recirculating water vacuum pump, and the obtained capsaicin extract (CAP) was stored at 4 °C.

2.3. Characterization of SA/SPI/CTS/CAP/Ag Gel

Fourier transform infrared spectroscopy (FT-IR) was applied to measure SA/SPI/CTS/CAP/Ag gel over 500–4000 cm^{-1}.

2.4. Antibacterial Property

The antibacterial properties of the antibacterial materials were tested using *E. coli* ATCC 25922, *S. aureus* ATCC 6538, and *P. aeruginosa* ATCC 9027 as experimental bacteria. All glassware used for antibacterial experiments was sterilized via high-pressure sterilization (121 °C, 20 min). The antibacterial activity of the materials was determined using the plate count method, and the antibacterial effect of the materials was evaluated via the well diffusion method. The bacterial suspension was diluted to 10^6 CFU/mL, and 100 μL of the bacterial suspension was evenly spread on the LB solid medium. A hole with a diameter of 9 mm was drilled on the LB solid medium covered with bacterial suspension. Then, 0.10 g (dry weight) of the CTS/SPI/Ag/CAP gel was added to the hole and incubated at 37 °C for 1 day. Then, the size of the inhibition zone was measured, and the antibacterial activity of the material was evaluated. The experimental data were recorded, and the antibacterial rate was given as shown in Equation (1):

$$\text{Antibacterial rate } (\%) = \frac{B0 - B1}{B0} \times 100 \quad (1)$$

where B0 represents the colony number without inhibition, and B1 represents the colony number after inhibition.

2.5. SA/SPI/CTS/CAP/Ag Gel Preparation

Here, 1 g of CTS was added to 49 mL of deionized water along with 1 mL of glacial acetic acid and stirred to form a 2 wt% CTS solution. Then, 0.5 g of SPI and 1 g of SA were added to 50 mL of deionized water and then stirred in an 80 °C water bath until dissolved to create an SPI-SA solution. The CTS solution was then poured into the SPI-SA solution and stirred evenly, followed by the addition of 0.3 g of boric acid and 0.05 g of polyvinyl pyrrolidone for crosslinking for 30 min. Subsequently, 0.05 g of silver nitrate was added and dissolved, and then 5 mL of capsaicin was added for a light-avoiding reduction reaction, which was stirred for 8 h until the reduction reaction was complete. After the

reaction was complete, the mixture was dripped into a 10 wt% calcium chloride solution to form a gel state (Figure 1). The gel was then removed, rinsed twice with deionized water, dried in a 60 °C oven, and stored in a sealed container to yield SA/SPI/CTS/CAP/Ag gel.

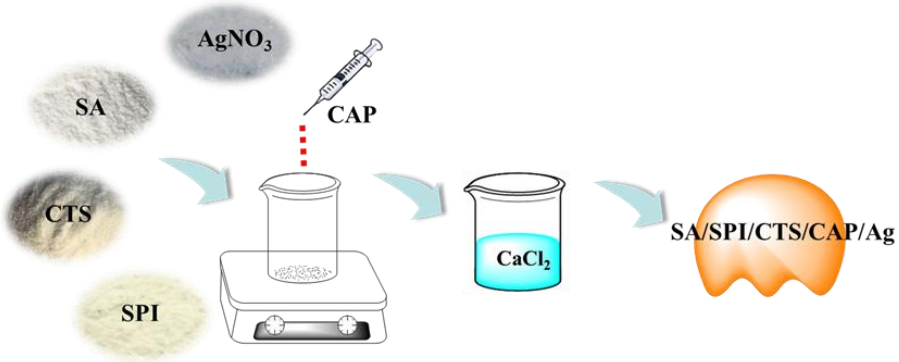

Figure 1. Preparation of the SA/SPI/CTS/CAP/Ag gel.

2.6. Optimization of Gel Preparation Method and the Influence of Ag and CTS Dosage in SA/SPI/CTS/CAP/Ag Gel on Antibacterial Effect

Gels containing different components (S: SPI; C: CTS; A: Ag; L: CAP) were prepared: S-C-L gel (without Ag ions but with other components), S-C-A gel (without capsaicin but with other components), S-A-L gel (without chitosan but with other components), and S-C-A-L gel (with all components). The antibacterial activity of these gels with different added components was evaluated using the diffusion method to assess their antimicrobial performance and determine the optimal combination of materials [28]. The antibacterial test was conducted on SA/SPI/CTS/CAP/Ag gels prepared with different concentrations of Ag (A content: 0.001–0.4 wt%) and CTS (C content: 0.5–4.0 wt%), and the influence of Ag and CTS content on the antibacterial effect was observed.

2.7. Effect of C/CTS/PVA/CNF Hydrogel Dosage and Incubation Time

Dosage and time optimization experiments were conducted with *P. aeruginosa*, *S. aureus*, and *E. coli* as the test bacteria. According to the plate counting method [29], different doses of gel (0.1, 0.2, 0.3, 0.4, and 0.5 g/L) were separately added to the physiological saline solution with a bacterial suspension concentration of 10^8 CFU/mL. The antibacterial gel was mixed in the bacterial suspension and incubated in a constant temperature shaker at 37 °C. Samples were taken every hour within 5 h, and 0.1 mL of the supernatant was diluted and spread on a plate. The antibacterial activity was detected via the plate counting method.

2.8. Antibacterial Reusability and Stability

The reusability of SA/SPI/CTS/CAP/Ag gel is an important aspect in practical applications [30]. The antibacterial activity of the gel against *P. aeruginosa*, *S. aureus*, and *E. coli* was tested in physiological saline. The gel was placed into a physiological saline solution with a bacterial suspension concentration of 10^8 CFU/mL for 6 h of bacterial inhibition, followed by the evaluation of the antibacterial performance of the gel after repeated use and a certain number of days using the plate counting method. Then, 0.1 g (dry weight) of SA/SPI/CTS/CAP/Ag gel was added to 50 mL of bacterial suspension (10^8 CFU/mL). After 1 h of antibacterial treatment, the bacterial content in the suspension was detected via the plate spreading method. After each antibacterial test, the gel was cleaned and dried for the next test. After 10 batches of antibacterial experiments, the antibacterial effects of the gel on the three types of bacteria were recorded and analyzed.

The stability of SA/SPI/CTS/CAP/Ag gel was another important characteristic of antibacterial materials [31]. The prepared SA/SPI/CTS/CAP/Ag gel was stored indoors, and

its antibacterial performance was tested on different days (5–45 d). The antibacterial results were recorded and analyzed each time to evaluate the stability of the antibacterial material.

2.9. Milk Antibacterial Simulation Experiment

In the preparation process, plastic Petri dishes were sterilized in an ultraviolet sterilizer for 20 min, and then 20 mL of milk was poured into each Petri dish. The prepared gel (0.3 g) was placed in each Petri dish. The Petri dishes were sealed with tape for 24 h to ensure that the antibacterial substances in the gel migrate into the milk. The sealing tape was then removed and stored at room temperature for 14 days. The appearance and smell of the milk were recorded daily during these 14 days.

2.10. Swelling Ratio, Water Loss, Moisture Adsorption, Moisture Content and of SA/SPI/CTS/CAP/Ag Gels

The swelling behavior of the gel materials in water is one of the main methods to characterize their properties [32,33]. SA/SPI/CTS/CAP/Ag gels containing different amounts of SPI (0.5–3 wt%) were taken separately, each weighing 0.1 g (dry weight), for the swelling experiment. The gels were placed in deionized water (with the gel fully immersed). Within 2 h, the gel was removed every 10 min, the surface water was wiped off with filter paper, and then it was weighed to record the changes in the mass of the gel. The expansion ratio was calculated as shown in Equation (2):

$$\text{Expansion ratio (\%)} = \frac{\text{W2} - \text{W1}}{\text{W1}} \times 100 \quad (2)$$

where W2 represents the pellet weight after treatment, and W1 represents pellet weight before treatment.

SA/SPI/CTS/CAP/Ag gels with different SPI contents (0.5–3 wt%) were prepared, dried, and set aside. Then, 0.1 g (dry weight) of wet gel was evaporated in a 60 °C oven for 1, 2, 3, 4, 5, 6, 8, 10, 20, and 30 min, then taken out and weighed to record the mass loss. The effect of SPI on the dehydration rate of SA/SPI/CTS/CAP/Ag gel was studied. The water loss rate of the hydrogels was calculated as shown in Equation (3):

$$\text{Water loss rate (\%)} = \frac{\text{M1} - \text{M2}}{\text{M1}} \times 100 \quad (3)$$

where M2 indicates the gel bead weight after treatment, and M1 represents the gel bead weight before treatment.

Moisture adsorption and water content are among the key indicators for evaluating the gel during daily storage. A 0.10 g sample of the gel is placed in a light-avoiding corner, and its weight was measured every 24 h. Over a span of 7 days, the morphological changes of the gel with different SPI concentrations were observed, and their water content was determined. The water content of the gel under varying SPI concentrations was measured to assess the moisturizing performance of the SA/SPI/CTS/CAP/Ag gel.

2.11. Degradation of SA/SPI/CTS/CAP/Ag Gels

Good degradation performance is a reflection of the environmental friendliness and energy conservation of gel materials [34]. The prepared SA/SPI/CTS/CAP/Ag gel was embedded in natural soil without adding any enzymes. The temperature and humidity were maintained at 37 °C and 80%, respectively. Every 5 days, over a period of 45 days, samples were taken from the soil, rinsed with water to remove dirt, and photographed to record the morphological characteristics of the gel. After drying in a constant-temperature drying oven, the weight of the gel before and after embedding was measured, and the degradation rate was calculated using the formula as a basis for evaluating the biodegradation performance of the gel.

The degradation rate (DR) formula is shown in Equation (4):

$$\mathrm{DR}\ (\%) = \frac{\mathrm{W0} - \mathrm{W1}}{\mathrm{W0}} \times 100 \quad (4)$$

where W0 and W1 are the weight of the sample before and after being buried.

2.12. Dye Adsorption with SA/SPI/CTS/CAP/Ag Gels

Here, 5 mL of the dye solutions [malachite green (2.5 g/L), Congo Red (2.5 g/L), methyl orange (0.5 g/L), and methylene blue (1.0 g/L) were each mixed with SA/SPI/CTS/CAP/Ag gel (0.10 g) and placed in a constant-temperature shaker at 25 °C with a rotation speed of 160 rpm. After oscillating for 24 h, a fixed sampling was performed. The extracted samples were diluted and separated in a centrifuge (8000 rpm) for 2 min. The absorbance of the supernatant was measured using a UV-visible spectrophotometer [35].

The adsorption (mg/g) of C/CTS/PVA/CNF hydrogel under balance was defined as shown in Equation (5):

$$q_e = \frac{(C_0 - C_e)V}{M} \quad (5)$$

where C_0 (mg/L) is the initial dye concentration. C_e (mg/L) is the equilibrium dye content. V (L) represents the dye solution volume. M (g) represents the mass of carbon aerogel. q_e (mg/g) represents the capacity of equilibrium adsorption.

The equations representing the pseudo-first-order kinetic model and pseudo-second-order kinetic model were denoted as shown in Equations (6) and (7)

$$q_t = q_e(1 - \exp(-k_1 t)) \quad (6)$$

$$q_t = \frac{k_2 q_e^2 t}{1 + k_2 q_e t} \quad (7)$$

where q_t (mg/g) is the adsorption amount when the adsorption time is t (h). q_e (mg/g) is the adsorption amount when the adsorption equilibrium is reached. k_1 and k_2 are the rates of the pseudo-first-order and pseudo-second-order dynamics mode.

3. Result and Discussion

3.1. Characterization of SA/SPI/CTS/CAP/Ag Gel

FTIR can be used to investigate the presence of specific chemical functional groups in materials and explore the molecular scale interactions between CTS, SA, Ag, and SPI (Figure 2a). The peak around 3420 cm^{-1} was associated with the hydrogen bonding interaction among the -OH groups of CTS and the Ag matrix [36]. The peak near 2927 $cm^{-1}$was ascribed to the stretching and bending vibrations of C-H [37]. The peaks about 1433 cm^{-1} and 1342 cm^{-1} indicated C-C stretching vibrations [38]. The presence of the peak at 1021 cm^{-1} suggested interactions between C-O-Ag [39]. At 819 cm^{-1}, there were weak absorption peaks related to C-H bending vibrations and -OH rotations [40].

X-ray diffraction (XRD) measurements were performed on the S/C/L and S/C/A/L gels (Figure 2b). The observed diffraction peak positions at 38.32°, 44.56°, 64.52°, and 76.36° matched those of silver. The results revealed a significant amount of silver in the antimicrobial gel, confirming the successful synthesis of the S/C/A/L gel.

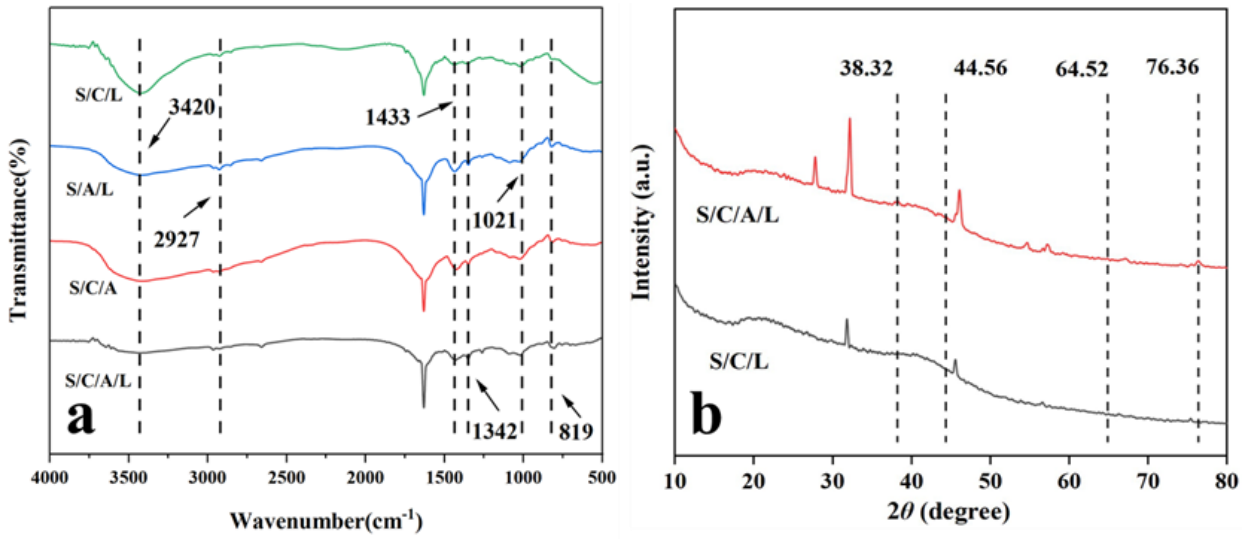

Figure 2. FT-IR spectra of S/C/L gels, S/A /L gels, S/C/A gels, and S/C/A/L gels (**a**), XRD patterns of S/C/L and S/C/A/L gels (**b**).

3.2. Antimicrobial Property

3.2.1. Optimization of Gel Preparation Method and the Influence of Ag and CTS Dosage in SA/SPI/CTS/CAP/Ag Gel on Antibacterial Effect

The materials used to prepare gel beads and the dosage of antimicrobial substances may affect the antibacterial activity [41]. The experimental data showed that, under the same experimental conditions, the S-C-L gel material without Ag ions had the weakest inhibitory effect on the three types of bacteria. The S-C-A-L gel material with all four materials added had the best antibacterial effect, and the S-A-L gel material without chitosan and the S-C-L gel material without capsaicin had moderate antibacterial effects (Figure 3a). The negative charge on the bacterial cell membrane interacted with the positively charged amines on CTS, disrupting the cell membrane. AgNPs enter the cell and affect microbial oxidative stress (ROS), leading to cell leakage and bacterial inactivation [42,43]. In S-C-A-L gels, the bonding interaction between CTS and SA might form a network-like adhesive structure, serving as a channel for the release of silver ions, thereby enhancing the antibacterial effect.

As illustrated in Figure 3b, with the increase in the dose of silver ions, the inhibitory effect of the gel on bacteria became stronger. The antibacterial activity was the strongest when silver ions were at 0.05 g/L. When the dosage reached a certain amount, AgNPs embedded in the S-C-A-L gel restricted the release of AgNPs, reducing the antibacterial capabilities. When the CTS dosage was 10 g/L, the antibacterial effect of the S-C-A-L gel reached its peak (Figure 3c). At the high loading of CTS, the network structure formed by CTS and SA became compact and dense, which influenced the release of AgNPs and significantly impacted the material's inhibitory capacity [44].

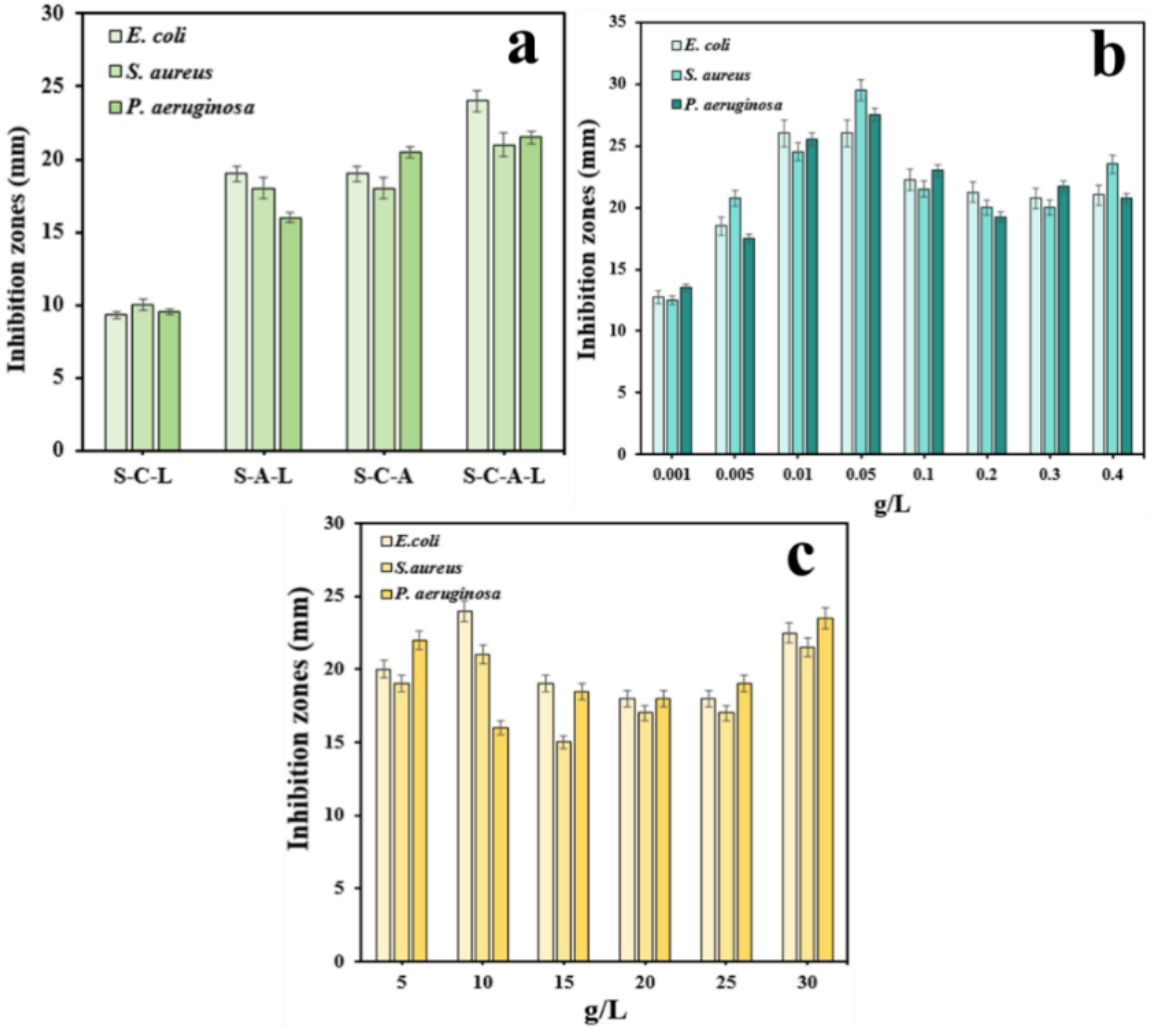

Figure 3. Antibacterial effect of gels prepared from different materials (S/C/L, S/A/L, S/C/A, and S/C/A/L) (**a**), C–Ag dosage (0.001,0.005,0.01, 0.05, 0.1, 0.2, 0.3, and 0.4 g/L) (**b**), chitosan dosage (5, 10, 15, 20, 25, and 30 g/L) (**c**).

3.2.2. Effect of SA/SPI/CTS/CAP/Ag Gel Dosage and Incubation Time

Increasing the dosage of antibacterial material and gradually extending the release time of the material can enhance its antibacterial effect [45]. As shown in Figure 4, with an increase in dosage and the prolongation of antibacterial time, the antibacterial efficiency underwent significant changes. *E. coli* is a common Gram-negative bacterium and a part of the gut flora [46]. It is a common microorganism in the intestines of humans and other mammals. By increasing the dosage of SA/SPI/CTS/CAP/Ag gel, the antibacterial effect was significantly enhanced within 1 h (Figure 4a). However, after 2 h, the antibacterial effect tended to stabilize. After 3 h of inhibition, the inhibition rate basically reached 100%. Increasing the gel dosage at this point did not further enhance the antibacterial effect. In some studies of composite gels, the antibacterial rate was less than 100% after 3 h with 0.8 g/L of antibacterial material [45]. In this study, the inhibition rate of 0.2 g/L SA/SPI/CTS/CAP/Ag gel was 100% within 2 h.

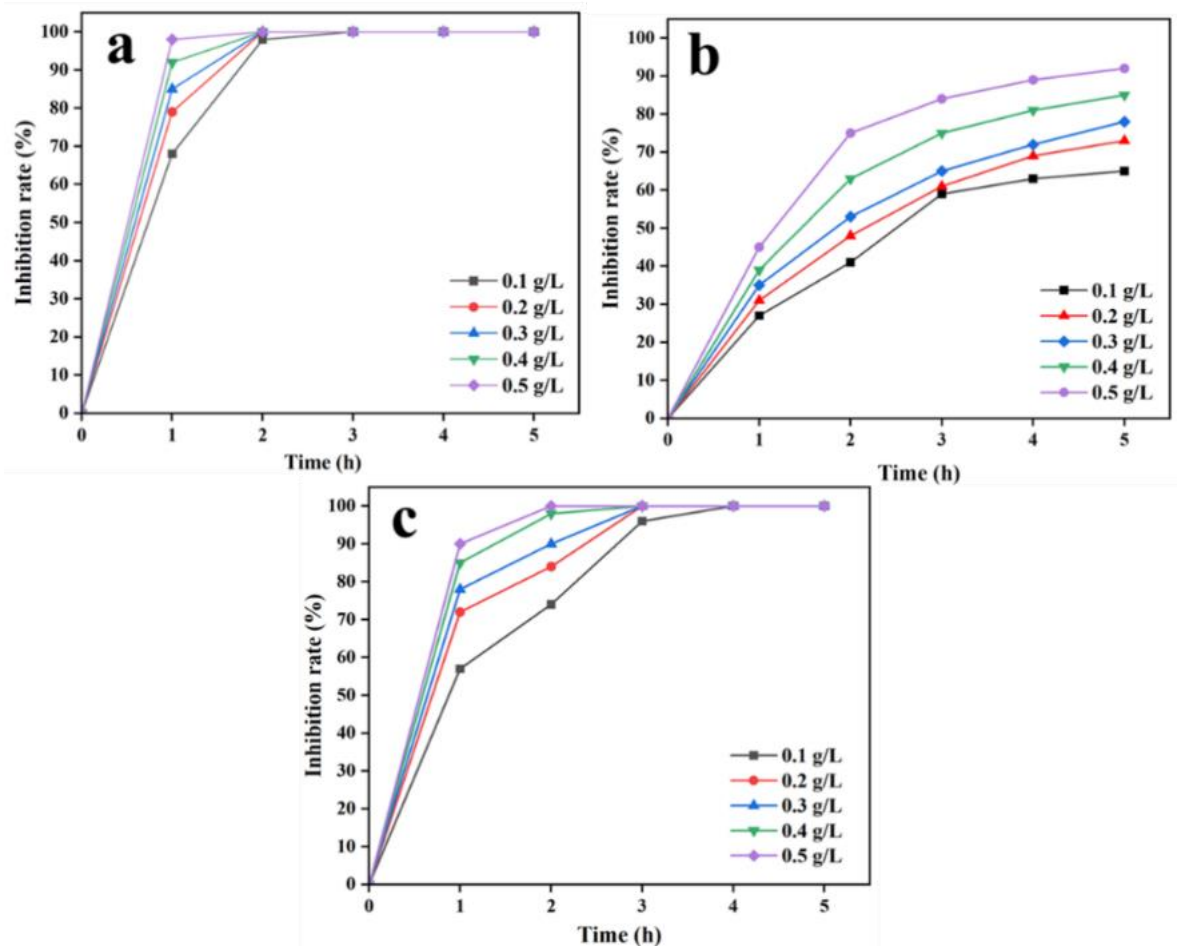

Figure 4. Antibacterial activity against *E. coli* (**a**), *S. aureus* (**b**), and *P. aeruginosa* (**c**) was observed in SA/SPI/CTS/CAP/Ag gel at different dosages (0.1, 0.2, 0.3, 0.4, and 0.5 g/L) and time (1.0, 2.0, 3.0, 4.0, and 5.0 h).

S. aureus is a significant pathogen capable of causing various infections, ranging from skin infections to severe visceral organ infections [47]. As shown in Figure 4b, with the increase in action time and the dosage of SA/SPI/CTS/CAP/Ag gel, the inhibition rate gradually increased, reaching its maximum intensity within 3 h, then stabilized, and the inhibition rate gradually increased at a slower pace. When the dosage of SA/SPI/CTS/CAP/Ag L gel reached > 0.5 g/L, the inhibition rate was greater than 90% after 5 h, indicating that the SA/SPI/CTS/CAP/Ag gel had excellent antibacterial activity against *S. aureus*.

P. aeruginosa is a multi-drug-resistant strain that is resistant to multiple antibiotics [48]. This would make it difficult to treat *P. aeruginosa* infections and increase the risk of treatment failure and serious complications. When the gel dosage was 0.4 g/L and the action time reached 3 h, the inhibition rate reached 100% (Figure 4c). Within 3 h, the antibacterial effect of the gel reached its maximum. When the antibacterial time exceeded 3 h, the antibacterial effect gradually increased steadily, and increasing the gel dosage no longer significantly enhanced the antibacterial effect.

Overall, the above results indicated that the SA/SPI/CTS/CAP/Ag gel exhibited significant antibacterial activity against both Gram-positive and Gram-negative bacteria, especially remarkable inhibitory effects against *E. coli*. Even at low dosages, the gel demonstrated excellent antibacterial activity during prolonged inhibition.

3.2.3. Stability and Reusability of SA/SPI/CTS/CAP/Ag Gel

The actual application scenarios of antibacterial materials are complex and varied. The stability and repeatability of antibacterial gels are considered important factors for adapting to different environments. The high stability of antibacterial gel can reduce the application cost and reduce the waste of resources. As shown in Figure 5a, the SA/SPI/CTS/CAP/Ag gel exhibited long-term stable antibacterial performance. The inhibitory effect of the SA/SPI/CTS/CAP/Ag gel was weakened after 30 days, but even after 40 days, the inhibition rate still remained above 90%. In some studies of antibacterial materials, the antibacterial rate of the gel prepared after 30 days dropped below 80% [49]. As shown in Figure 5b, the antibacterial effect began to decline after seven repeated antibacterial tests. This was due to the loss of antibacterial compounds caused by the repeated use of the SA/SPI/CTS/CAP/Ag gel. However, even after ten antibacterial cycles, the inhibition rate still remained above 90%. However, the durability of natural antibacterial materials in some studies was relatively weak, and the antibacterial effect significantly decreased after five tests [50]. These results demonstrated that the SA/SPI/CTS/CAP/Ag gel exhibited good stability and repeatability.

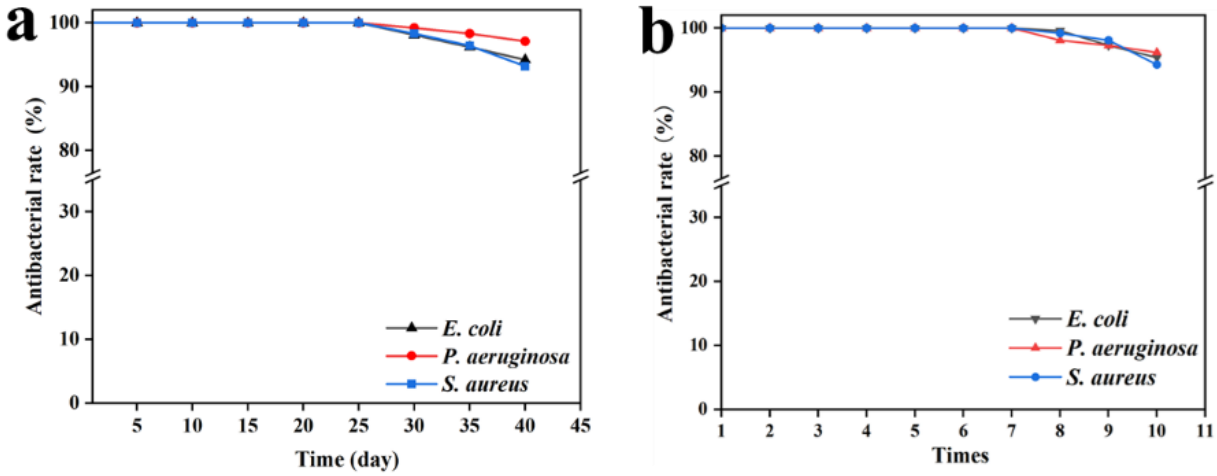

Figure 5. Antibacterial effect images of SA/SPI/CTS/CAP/Ag gels prepared on different days (5, 10, 15, 20, 25, 30, 35, and 40 days) (**a**), repetitive antibacterial properties (1, 2, 3, 4, 5, 6, 7, 8, 9, and 10 times) (**b**).

3.2.4. Milk Antimicrobial Simulation Test

Milk is a food that is extremely prone to spoilage and susceptible to bacterial contamination [51]. As shown in Figure 6, on the 6th day, the milk samples of S-C-L, S-A-L, and S-C-A gels showed a small amount of solid milk residue and yellow bacterial colonies on the surface of the milk, accompanied by a slight foul smell. No significant changes were observed in the S-A-L gel samples. On the 9th day of the experiment, the smell of the S-C-A-L gel sample did not change, and the milk was light brown; all other three samples showed obvious spoilage, an increase in solid milk residue, and a large amount of growth of yellow colonies, with a strong acidic smell. S-A-L and S-C-A gel samples showed solid milk residue and an obvious spoilage smell, and S-C-L gel samples were noticeably dried into chunks, and yellow colonies appeared. On the 14th day, S-C-L gel, S-A-L gel, and S-C-A gel samples all showed a large amount of solid yellow milk residue, accompanied by a strong acidic smell. There were many bacterial colonies on the surface of the milk. In contrast, the S-C-A-L gel sample had a slightly acidic smell, no large number of bacterial colonies was found, and the color of the milk turned brown. This might be due to the presence of unsaturated fatty acids in milk. These unsaturated fatty acids might be easily oxidized by oxygen in the air, resulting in the production of oxidation compounds and the browning of milk [52,53].

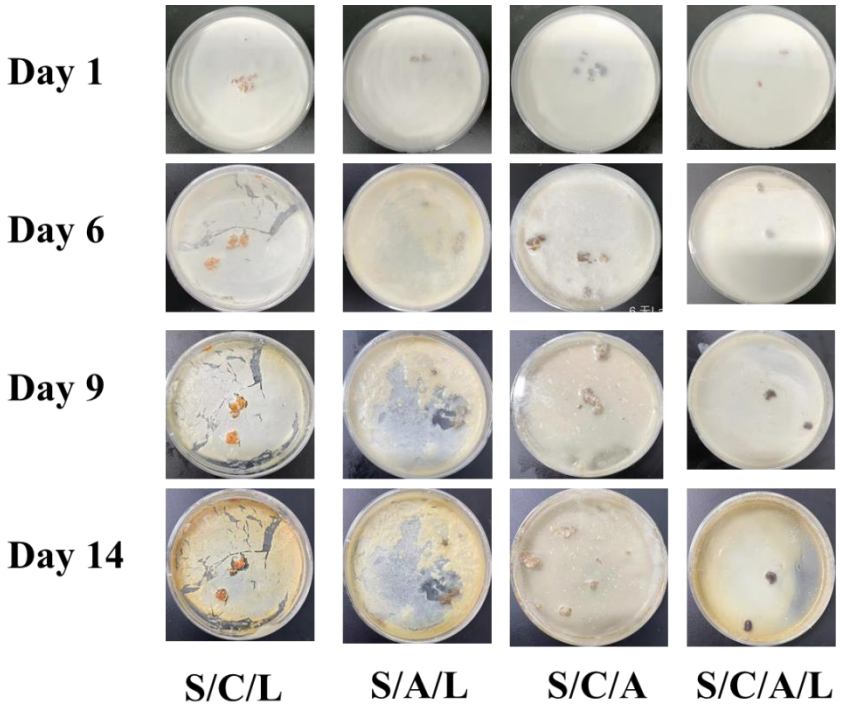

Figure 6. Microbial growth in fresh milk containing S/C/L, S/A/L, S/C/A, and S/C/A/L gels after 14 days.

Accordingly, the antibacterial test results of milk were consistent with the above-mentioned antibacterial results. The S-C-A-L gel demonstrated excellent antibacterial ability, as the antibacterial substances in the hydrogel could inhibit the growth of various bacteria. Hence, the S-C-A-L gel could significantly extend the shelf life of milk.

3.2.5. Synergistic Antibacterial Mechanism of SA/SPI/CTS/CAP/Ag Gel

The gel system was constructed with SA and CTS, and SPI was added to stabilize the network structure and provide a carrier for AgNPs. When the gel was immersed in water, the hydrophilic groups of CTS and SPI readily absorbed water [54], leading to pore expansion and promoting the release of AgNPs and -NH_2 in the SA/SPI/CTS/CAP/Ag gel. AgNPs and -NH_2 might penetrate the cellular membrane, causing an exchange of internal and external charges, leading to the leakage of cell contents. Additionally, AgNPs and -NH_2 might enter the cell wall and subsequently disrupt ion transportation channels [55]. The synthesis of enzymes might be disrupted, and proteins would be destroyed, resulting in bacterial inactivation [51,56]. In this study, a crosslinked network structure gel was constructed, and AgNPs were fully loaded into the network structure. During the antibacterial process, good hydrophilicity and swelling properties expanded the apparent area between bacteria and gels, promoting the synergistic antibacterial action of AgNPs and CTS (Figure 7). The simple preparation of the SA/SPI/CTS/CAP/Ag gel could enhance the environmental friendliness and application potential of antibacterial materials, making it a promising candidate for microbial water treatment applications.

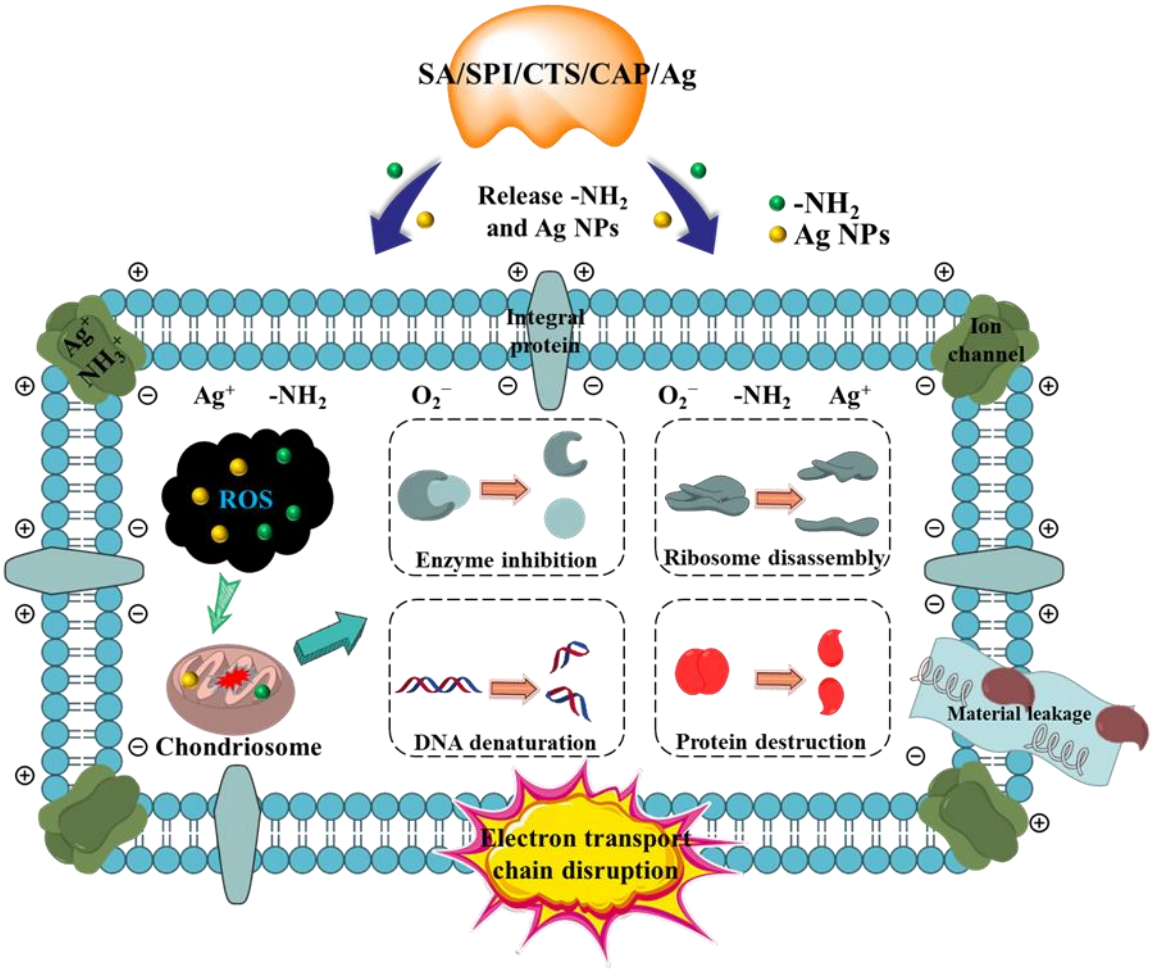

Figure 7. Synergistic antibacterial mechanism of SA/SPI/CTS/CAP/Ag gels.

3.3. Swelling Ratio, Water Loss, Moisture Adsorption, Moisture Content and of SA/SPI/CTS/CAP/Ag Gel

The swelling rate of the gel is a key indicator characterizing its physical properties [57]. As shown in Figure 8a, over a certain period, the longer the SA/SPI/CTS/CAP/Ag gel material soaks in water, the higher the swelling rate. When the SPI content was 0.5–1.0%, the swelling rate of the gel increased with the increase in SPI dosage. When the SPI concentration was 1.0%, the swelling rate was the highest, approaching 300%. When the SPI content was 1.0–3.0%, the swelling rate decreased with the increase in SPI dosage. This was because SPI, as an enhancer, promoted the crosslinking of CTS and SA at low concentrations, leading to an increase in the structure of the gel pore and promoting gel swelling. However, too high SPI loading could cause the gel structure to be too dense, which would not be conducive to gel swelling.

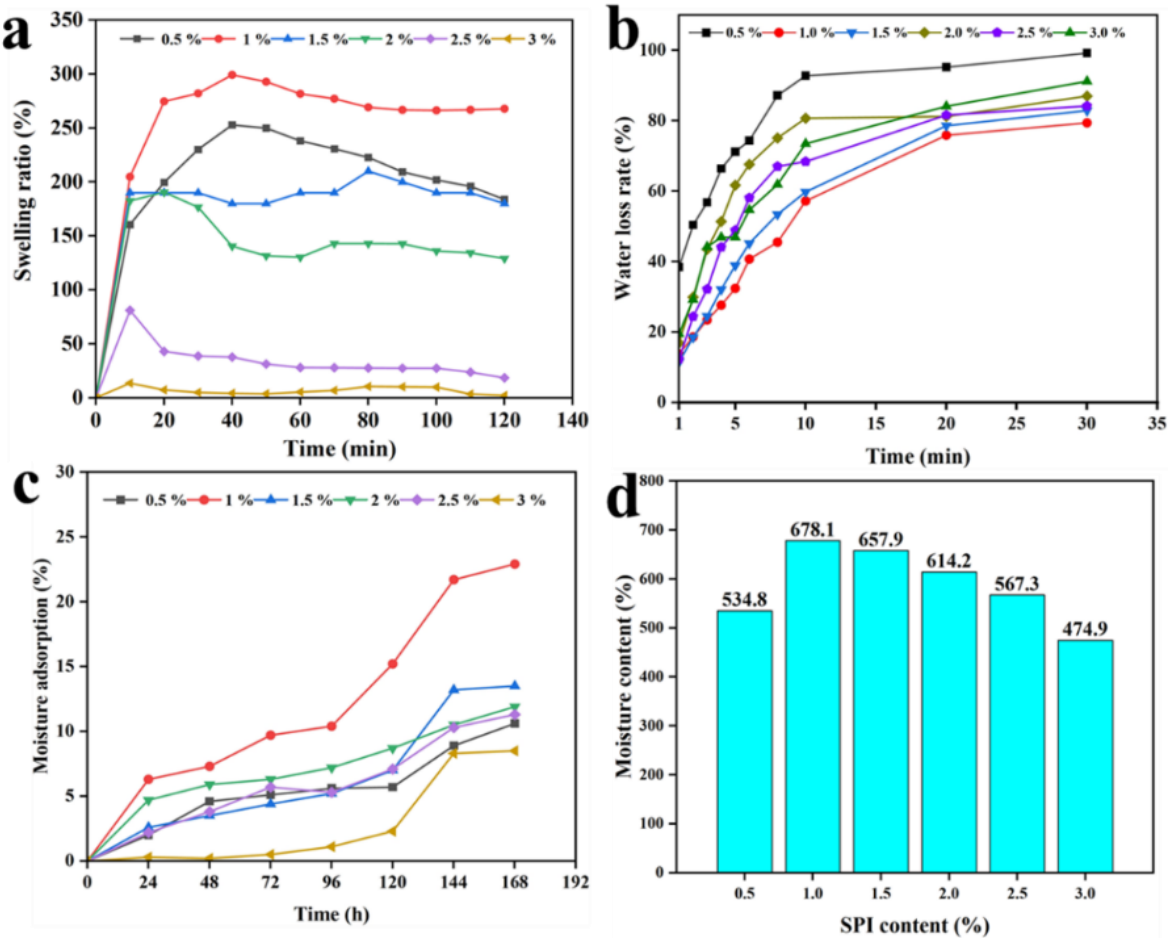

Figure 8. Swelling effect (**a**), water loss (**b**), moisture adsorption (**c**), and moisture content (**d**) images of different SPI dosage (0.5, 1.0, 1.5, 2.0, 2.5, and 3.0 wt%).

In the dehydration test experiment, as the exposure time of the SA/SPI/CTS/CAP/Ag gel in the oven increased, the water inside the hydrogel began to evaporate. SPI affected the crosslinking of CTS and SA, thereby affecting the water loss in the gel. Figure 8b shows the effect of SPI dosage on the gel water loss rate. Within a certain range of SPI concentration, the water loss rate of the gel gradually decreased as the SPI dosage increased. When the SPI concentration was 1.0%, the water loss rate of the gel was lowest. When the SPI concentration was 0.5%, the water loss rate approached 94% after drying for 30 min. When the concentration was 1.0% and 1.5%, the water loss rates were both below 80%. This indicated that the addition of an appropriate amount of SPI could significantly improve the water retention of the hydrogel.

Figure 8c,d shows that SPI concentration affects the moisture absorption rate and moisture content of the SA/SPI/CTS/CAP/Ag gel. When the SPI concentration was 1.0% and 1.5%, the moisture absorption rate of the gel still showed an increasing trend, even after 96 h, and the moisture absorption rate was significantly higher than that of the gel with concentrations of 0.5% and 3.0%. This indicated that an appropriate amount of SPI significantly enhanced the moisture absorption capability of the gel. In the moisture content test, the SA/SPI/CTS/CAP/Ag gel showed strong water retention. When the SPI concentration was greater than 1.0%, the moisture adsorption and moisture content of the gel decreased with the increase in SPI dosage. This was due to the impact of SPI concentration on the structural morphology and crosslinking strength of the gel, representing the typical diffusion of water in the networked, adhesive structure [58,59]. The results of the swelling rate, water loss rate, moisture absorption rate, and moisture

content tests showed that the SA/SPI/CTS/CAP/Ag gel had excellent physical properties, with a complex porous network structure that effectively controls water permeation.

3.4. SA/SPI/CTS/CAP/Ag Gel Degradation

Degradability is an important indicator for evaluating the performance of antimicrobial materials, reflecting the principle of environmental friendliness [60]. The hygroscopic property of SPI is beneficial for absorbing moisture from the soil, accelerating degradation. S-C-A-L and S-C-A gels had the highest degradation rate, reaching 96% (Figure 9). In S-A-L gel, the absence of CTS addition made the structure compact. It was difficult for water to permeate, and the gel degradation rate was greatly reduced. The degradation rate of the S-C-L gel was only 85%. When both CTS and silver ions were added simultaneously, the silver ions permeated into CTS, creating small pores. During the degradation process, the gel absorbed water and swelled, increasing the size of the pores, thereby enlarging the contact area and promoting the entry of microorganisms and oxygen. The degradation efficiency was significantly enhanced. S-C-A-L gel did not harm the environment during the antimicrobial process and was an environmentally friendly antimicrobial material with high market value.

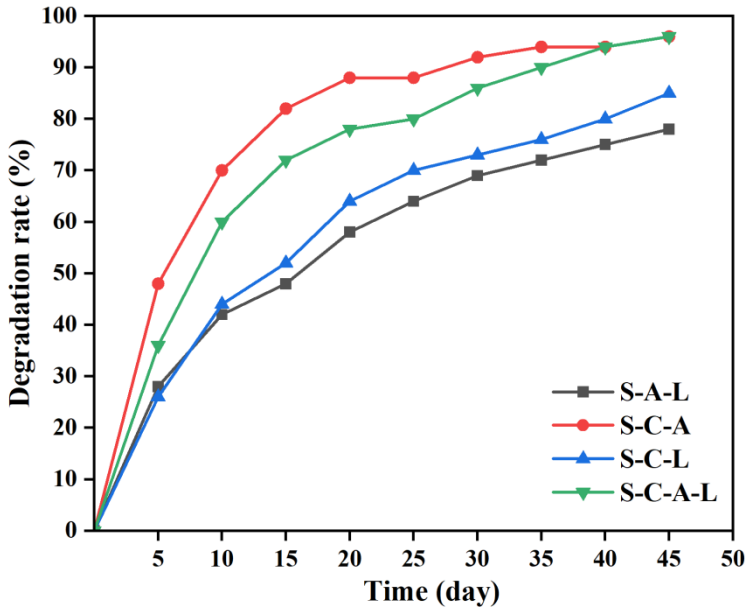

Figure 9. Degradation curve images of S/C/L, S/A /L, S/C/A, and S/C/A/L gels within 45 days.

3.5. SA/SPI/CTS/CAP/Ag Gel Dye Adsorption Properties

The adsorption results showed that the adsorption rates of MB, MG, and MO reached equilibrium around 4 h, while the adsorption rate of CR reached equilibrium around 6 h (Figure 10). This indicated that the pores inside the gel were filled with a large amount of dye during the adsorption process. The adsorption action of the gel was mainly achieved through electrostatic adsorption and physical adsorption. The charges in the gel would spark an electrostatic reaction with dye ions. Physical adsorption mainly involved the hydrogen bond interaction between hydroxyl and carboxyl groups with pollutant molecules. Data fitting showed that the gel had a significant affinity for MG, with a maximum adsorption capacity reaching 42.48 mg/g. This was comparable to the adsorption efficiency of some nanomaterials [61]. As shown in Table 1, the adsorption kinetics of SA/SPI/CTS/CAP/Ag gel could be well described by the pseudo-second-order equation, where the R^2 value of all four groups was 0.99, while the pseudo-first-order kinetics equation only had two groups with R^2 values of 0.99.

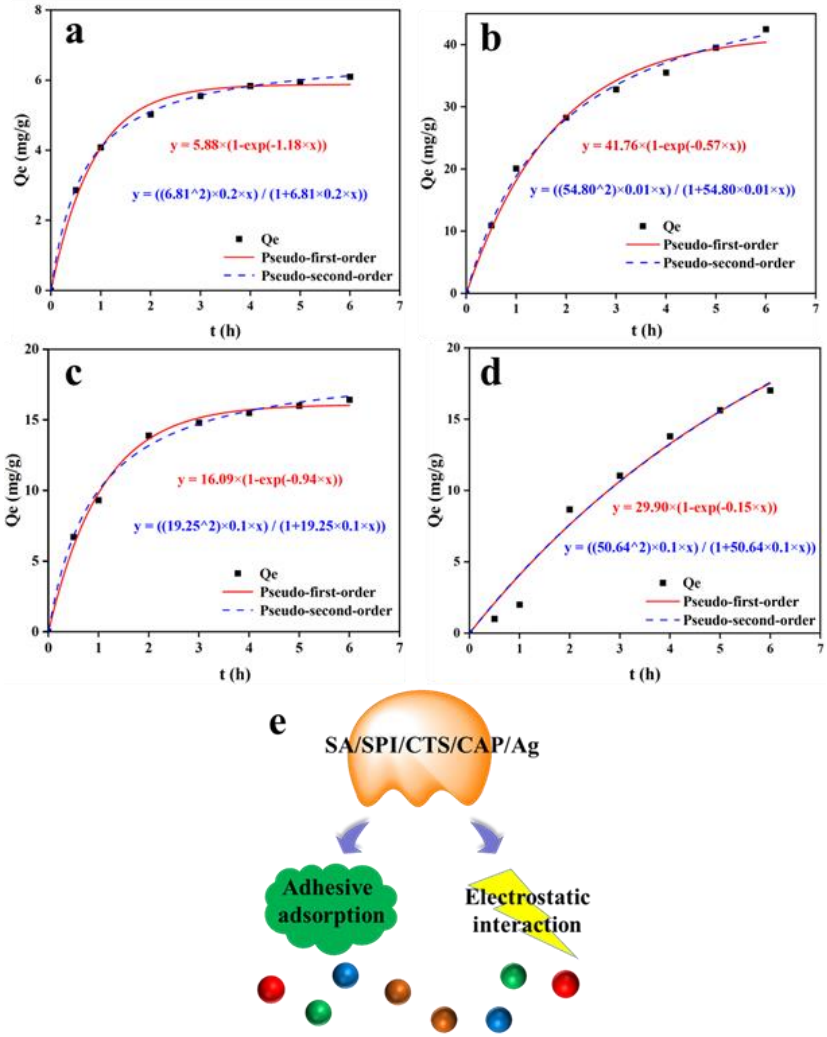

Figure 10. Kinetic fitting results for methylene blue (MB: 1 g/L) (**a**), malachite green (MG: 2.5 g/L) (**b**), methyl orange (MO: 1 g/L) (**c**), and Congo red (CR: 2.5 g/L) (**d**) adsorption onto SA/SPI/CTS/CAP/Ag gels. Dye adsorption mechanism (**e**).

Table 1. Kinetic parameters for the adsorption of dyes on SA/SPI/CTS/CAP/Ag gel.

Dye	$q_{e\ exp}$ (mg/g)	Pseudo-First-Order Model			Pseudo-Second-Order Model		
		$q_{e\ cal}$ (mg/g)	k_1 (min^{-1})	R^2	$q_{e\ cal}$ (mg/g)	k_2 (g/mg·min)	R^2
MB	6.10	5.87	1.18	0.99	6.12	0.22	0.99
MG	42.48	40.41	0.57	0.98	41.42	0.01	0.99
MO	16.42	16.03	0.94	0.98	16.68	0.05	0.99
CR	17.01	17.52	0.14	0.99	17.58	0.01	0.99

The equilibrium adsorption capacities ($q_{e\ cal}$) calculated by fitting the pseudo-first-order kinetic model for MB, MG, MO, and CR were 5.87, 40.41, 16.03, and 17.52 mg/g. According to the pseudo-second-order kinetic model, the calculated equilibrium adsorption capacities for MB, MG, MO, and CR were 6.12, 41.42, 16.68, and 17.58 mg/g. The maximum adsorption capacities ($q_{e\ exp}$) for MB, MG, MO, and CR were 6.10, 42.48, 16.42, and 17.01 mg/g. It could be seen that the fitting curve well matched the pseudo-second-order kinetic equation.

The reliability of the adsorption model was determined by the correlation coefficient R^2 of the curve (its value was close to 1), indicating strong correlation and high reliability [62]. Therefore, the pseudo-second-order kinetic equation could effectively describe the

entire adsorption process. The results of the adsorption experiments showed that the SA/SPI/CTS/CAP/Ag gel had good adsorption capacity for dyes, highlighting its application potential in various practical scenarios. The hydrogel had good antibacterial and adsorption properties and had extensive application value in the field of wastewater treatment and water purification.

4. Conclusions

This study adhered to the principles of green, environmental protection, and sustainable development, using natural products to prepare SA/SPI/CTS/CAP/Ag gel with antibacterial and dye adsorption capabilities. In the antibacterial experiment, the SA/SPI/CTS/CAP/Ag gel displayed good antibacterial performance. This was attributed to the porous hydrophobic structure of the gel promoting the release of silver ions and amines, playing a synergistic antibacterial effect of CTS and AgNPs. In the milk preservation simulation experiment, the SA/SPI/CTS/CAP/Ag gel significantly extended the shelf life of the milk. This was a strong exploration of the application of antibacterial gel materials in the field of food preservation. The large number of hydrophobic amino acid residues in SPI effectively improves the high swelling performance of the gel. In addition, the gel had a good adsorption capacity for dyes, with the highest adsorption capacity for malachite green being 42.48 mg/g. Therefore, this environmentally friendly and energy-saving antibacterial material represented a new exploration in the use and development of green energy.

Author Contributions: Conceptualization, Methodology, Data curation, Software, and Writing original draft, Z.Z., M.H., and K.S.; Supervision, Review, and revising manuscript, Y.H. and Y.L. All authors have read and agreed to the published version of the manuscript.

Funding: This research is supported by the project of Sci-Tech Support Plan (Agriculture) (No. TN202203).

Institutional Review Board Statement: Not applicable.

Informed Consent Statement: Not applicable.

Data Availability Statement: Data are contained within the article.

Acknowledgments: The authors thank the Analysis and Testing Center (Changzhou University) for analysis of samples with FT-IR.

Conflicts of Interest: Author Meizi Huang was employed by the company Jiangsu ShenQi Medicine Technology Co., Ltd. The remaining authors declare that the research was conducted in the absence of any commercial or financial relationships that could be construed as a potential conflict of interest.

References

1. Xu, J.; Xu, Z. China sewage treatment engineering issues assessment. *J. Clean. Prod.* **2022**, *377*, 134391.
2. He, Q.; Zhang, H.; Ma, M.; He, Y.; Jia, J.; Hu, Q.; Gong, Y. Critical assessment of protozoa contamination and control measures in mass culture of the diatom Phaeodactylum tricornutum. *Bioresour. Technol.* **2022**, *359*, 127460.
3. Abdelaziz, M.A.; Owda, M.E.; Abouzeid, R.E.; Alaysuy, O.; Mohamed, E.I. Kinetics, isotherms, and mechanism of removing cationic and anionic dyes from aqueous solutions using chitosan/magnetite/silver nanoparticles. *Int. J. Biol. Macromol.* **2023**, *225*, 1462–1475.
4. Gopalakrishnan, S.; Kannan, P.; Balasubramani, K.; Rajamohan, N.; Rajasimman, M. Sustainable remediation of toxic congo red dye pollution using bio based carbon nanocomposite: Modelling and performance evaluation. *Chemosphere* **2023**, *343*, 140206.
5. Li, X.; Xu, L.; Gao, J.; Yan, M.; Bi, H.; Wang, Q. Surface modification of chitin nanofibers with dopamine as efficient nanosorbents for enhanced removal of dye pollution and metal ions. *Int. J. Biol. Macromol.* **2023**, *253*, 127113.
6. Xie, L.; Zhang, Z.; He, Y. Antibacterial Effect of Polyvinyl Alcohol/Biochar–Nano Silver/Sodium Alginate Gel Beads. *Processes* **2023**, *11*, 2330.
7. Zhang, Z.; He, Y. Synthesis and Characteristics of a Fish Scale-Based Biochar–Nanosilver Antibacterial Material. *Processes* **2023**, *11*, 1992.
8. Noguchi, M.; Aizawa, R.; Nakazawa, D.; Hakumura, Y.; Furuhashi, Y.; Yang, S.; Ninomiya, K.; Takahashi, K.; Honda, R. Application of real treated wastewater to starch production by microalgae: Potential effect of nutrients and microbial contamination. *Biochem. Eng. J.* **2021**, *169*, 107973.

9. El-Sherbiny, G.M.; El-Nour, S.A.A.; Askar, A.A.; Mohammad, N.H.; Hammad, A.A. Solar radiation-induced synthesis of bacterial cellulose/silver nanoparticles (BC/AgNPs) composite using BC as reducing and capping agent. *Bioprocess Biosyst. Eng.* **2021**, *45*, 257–268.
10. Hariram, M.; Vivekanandhan, S.; Ganesan, V.; Muthuramkumar, S.; Rodriguez-Uribe, A.; Mohanty, A.; Misra, M. Tecoma stans flower extract assisted biogenic synthesis of functional Ag-Talc nanostructures for antimicrobial applications. *Bioresour. Technol. Rep.* **2019**, *7*, 100298.
11. Poornima, H.; Srivastava, A.; Sharma, V.K.; Harikrishna; Kundu, A.; Singh, K.; Parihar, B.; Mangal, M. Assessing the retention of capsaicin and capsanthin compounds in chilli (*Capsicum annuum* L.) genotypes during storage. *J. Food Compos. Anal.* **2024**, *127*, 105948.
12. Mansalai, P.; Intanon, N.; Payaka, A.; Wattanalaorsomboon, S.; Chinvongamorn, C.; Sansenya, S. Inhibition potential against acetylcholinesterase of commercial and extracts of capsaicin and dihydrocapsaicin by in vitro and in silico studies. *Process. Biochem.* **2024**, *136*, 341–350.
13. Nolden, A.A.; Lenart, G.; Spielman, A.I.; Hayes, J.E. Inducible desensitization to capsaicin with repeated low-dose exposure in human volunteers. *Physiol. Behav.* **2024**, *275*, 114447.
14. Hunter, S.R.; Beatty, C.; Dalton, P.H. More spice, less salt: How capsaicin affects liking for and perceived saltiness of foods in people with smell loss. *Appetite* **2023**, *190*, 107032.
15. Pan, H.; Jiang, B.; Chen, J.; Jin, Z. Blend-modification of soy protein/lauric acid edible films using polysaccharides. *Food Chem.* **2014**, *151*, 1–6.
16. Feng, K.; Hung, G.-Y.; Yang, X.; Liu, M. High-strength and physical cross-linked nanocomposite hydrogel with clay nanotubes for strain sensor and dye adsorption application. *Compos. Sci. Technol.* **2019**, *181*, 107701.
17. Zolfagharian, S.; Zahedi, P.; Ardestani, M.S.; Khatibi, A.; Jafarkhani, S. Sodium alginate/xanthan-based nanocomposite hydrogels containing 5-fluorouracil: Characterization and cancer cell death studies in presence of halloysite nanotube. *J. Ind. Eng. Chem.* **2023**, *120*, 374–386.
18. Haleem, A.; Wu, F.; Ullah, M.; Saeed, T.; Li, H.; Pan, J. Chitosan functionalization with vinyl monomers via ultraviolet illumination under cryogenic conditions for efficient palladium recovery from waste electronic materials. *Sep. Purif. Technol.* **2024**, *329*, 125213.
19. Haleem, A.; Wu, F.; Wang, W.; Ullah, M.; Li, H.; Shah, A.; Pan, J. Fast and effective palladium adsorption from electronic waste using a highly macroporous monolith synthesized via rapid UV-irradiation. *Sep. Purif. Technol.* **2024**, *331*, 125500.
20. Salama, H.E.; Aziz, M.S.A. Non-toxic chitosan-pyrazole adsorbent enriched with greenly synthesized zinc oxide nanoparticles for dye removal from wastewater. *Int. J. Biol. Macromol.* **2023**, *241*, 124632.
21. Rath, A.; Grisin, B.; Pallicity, T.D.; Glaser, L.; Guhathakurta, J.; Oehlsen, N.; Simon, S.; Carosella, S.; Middendorf, P.; Stegbauer, L. Fabrication of chitosan-flax composites with differing molecular weights and its effect on mechanical properties. *Compos. Sci. Technol.* **2023**, *235*, 109952.
22. Guan, X.; Zhang, B.; Li, D.; Ren, J.; Zhu, Y.; Sun, Z.; Chen, Y. Semi-unzipping of chitosan-sodium alginate polyelectrolyte gel for efficient capture of metallic mineral ions from tannery effluent. *Chem. Eng. J.* **2023**, *452*, 139532.
23. López-Maldonado, E.A.; Oropeza-Guzmán, M.T. Synthesis and physicochemical mechanistic evaluation of chitosan-based interbiopolyelectrolyte complexes for effective encapsulation of OLZ for potential application in nano-psychiatry. *Sustain. Chem. Pharm.* **2021**, *22*, 100456.
24. Zhao, T.; Li, X.; Gong, Y.; Guo, Y.; Quan, F.; Shi, Q. Study on polysaccharide polyelectrolyte complex and fabrication of alginate/chitosan derivative composite fibers. *Int. J. Biol. Macromol.* **2021**, *184*, 181–187.
25. Tang, C.-H. Nanostructured soy proteins: Fabrication and applications as delivery systems for bioactives (a review). *Food Hydrocoll.* **2019**, *91*, 92–116.
26. Rahman, M.M.; Netravali, A.N. High-performance green nanocomposites using aligned bacterial cellulose and soy protein. *Compos. Sci. Technol.* **2017**, *146*, 183–190.
27. Luna-Sánchez, J.; Jiménez-Pérez, J.; Carbajal-Valdez, R.; Lopez-Gamboa, G.; Pérez-González, M.; Correa-Pacheco, Z. Green synthesis of silver nanoparticles using Jalapeño Chili extract and thermal lens study of acrylic resin nanocomposites. *Thermochim. Acta* **2019**, *678*, 178314.
28. Zhao, H.; Li, X.; Zhang, L.; Hu, Z.; Zhong, L.; Xue, J. Preparation and bacteriostatic research of porous polyvinyl alcohol/biochar/nanosilver polymer gel for drinking water treatment. *Sci. Rep.* **2021**, *11*, 12205.
29. Tantray, J.A.; Mansoor, S.; Wani, R.F.C.; Nissa, N.U. Chapter 43—Pour plate method for bacterial colony counting. In *Basic Life Science Methods*; Tantray, J.A., Mansoor, S., Wani, R.F.C., Nissa, N.U., Eds.; Academic Press: Cambridge, MA, USA, 2023; pp. 177–179.
30. Kumar, A.; Negi, Y.S.; Bhardwaj, N.K.; Choudhary, V. Synthesis and characterization of methylcellulose/PVA based porous composite. *Carbohydr. Polym.* **2012**, *88*, 1364–1372.
31. Lin, D.; Kelly, A.L.; Maidannyk, V.; Miao, S. Effect of concentrations of alginate, soy protein isolate and sunflower oil on water loss, shrinkage, elastic and structural properties of alginate-based emulsion gel beads during gelation. *Food Hydrocoll.* **2020**, *108*, 105998.
32. Zhang, S.; Liu, C.; Yuan, Y.; Fan, M.; Zhang, D.; Wang, D.; Xu, Y. Selective, highly efficient extraction of Cr(III), Pb(II) and Fe(III) from complex water environment with a tea residue derived porous gel adsorbent. *Bioresour. Technol.* **2020**, *311*, 123520.

33. Zeng, H.; Sun, S.; Xu, K.; Zhao, W.; Hao, R.; Zhang, J.; Li, D. Iron-loaded magnetic alginate-chitosan double-gel interpenetrated porous beads for phosphate removal from water: Preparation, adsorption behavior and pH stability. *React. Funct. Polym.* **2022**, *177*, 105328.
34. Wang, Y.; Liu, D.; Liao, R.; Zhang, G.; Zhang, M.; Li, X. Study of adhesive self-degrading gel for wellbore sealing. *Colloids Surf. A Physicochem. Eng. Asp.* **2022**, *651*, 129567.
35. Zhang, Z.; He, Y.-C.; Liu, Y. Efficient antibacterial and dye adsorption by novel fish scale silver biochar composite gel. *Int. J. Biol. Macromol.* **2023**, *248*, 125804.
36. Xiang, X.; Yi, X.; Zheng, W.; Li, Y.; Zhang, C.; Wang, X.; Chen, Z.; Huang, M.; Ying, G.-G. Enhanced biodegradation of thiamethoxam with a novel polyvinyl alcohol (PVA)/sodium alginate (SA)/biochar immobilized Chryseobacterium sp H5, *J. Hazard. Mater.* **2023**, *443*, 130247.
37. Salunke, A.S.; Salunke, S.T.; Deokate, R.J.; Kale, B.B. Tuning of photoluminescence behavior of gold coated chitosan-polyvinyl alcohol binding with graphene quantum dots. *Mater. Today Proc.* **2022**, *62*, 1752–1757.
38. Wei, W.; Shang, N.; Zhang, X.; Liu, W.; Zhang, T.; Wu, M. A green 3-step combined modification for the preparation of biomass sorbent from waste chestnut thorns shell to efficient removal of methylene blue. *Bioresour. Technol.* **2022**, *360*, 127593.
39. Liang, W.; Zheng, J.; Saleh, A.S.; Zhao, W.; Liu, X.; Su, C.; Yan, M.; Ge, X.; Shen, H.; Ospankulova, G.; et al. Fabrication of biodegradable blend plastic from konjac glucomannan/zein/ PVA and understanding its multi-scale structure and physicochemical properties. *Int. J. Biol. Macromol.* **2023**, *225*, 172–184.
40. Xia, D.; Liu, Y.; Cheng, X.; Gu, P.; Chen, Q.; Zhang, Z. Temperature-tuned fish-scale biochar with two-dimensional homogeneous porous structure: A promising uranium extractant. *Appl. Surf. Sci.* **2022**, *591*, 153136.
41. Anusuya, N.; Pragathiswaran, C.; Mary, J.V. A potential catalyst—TiO_2/ZnO based chitosan gel beads for the reduction of nitro-aromatic compounds aggregated sodium borohydride and their antimicrobial activity. *J. Mol. Struct.* **2021**, *1236*, 130197.
42. Wang, D.; Zhao, L.; Ma, H.; Zhang, H.; Guo, L.-H. Quantitative Analysis of Reactive Oxygen Species Photogenerated on Metal Oxide Nanoparticles and Their Bacteria Toxicity: The Role of Superoxide Radicals. *Environ. Sci. Technol.* **2017**, *51*, 10137–10145.
43. Xie, H.; Ouyang, K.; Zhang, L.; Hu, J.; Huang, S.; Sun, W.; Xiong, H.; Zhao, Q. Chitosan/rice hydrolysate/curcumin composite film: Effect of chitosan molecular weight. *Int. J. Biol. Macromol.* **2022**, *210*, 53–62.
44. Janani, B.; Okla, M.K.; Abdel-Maksoud, M.A.; AbdElgawad, H.; Thomas, A.M.; Raju, L.L.; Al-Qahtani, W.H.; Khan, S.S. CuO loaded ZnS nanoflower entrapped on PVA-chitosan matrix for boosted visible light photocatalysis for tetracycline degradation and anti-bacterial application. *J. Environ. Manag.* **2022**, *306*, 114396.
45. Hu, Z.; Zhang, L.; Zhong, L.; Zhou, Y.; Xue, J.; Li, Y. Preparation of an antibacterial chitosan-coated biochar-nanosilver composite for drinking water purification. *Carbohydr. Polym.* **2019**, *219*, 290–297.
46. Zhang, J.; Su, P.; Xu, T.; Yuan, L.; Qiao, M.; Yang, B.; Zhao, X. Comprehensive study on the role of reactive oxygen species and active chlorine species on the inactivation and subcellular damage of *E.coli* in electrochemical disinfection. *Sep. Purif. Technol.* **2023**, *304*, 122408.
47. Saha, S.; Malik, M.; Qureshi, M. Study of Synergistic Effects of Antibiotics And Triangular Shaped Silver Nanoparticles, Synthesized Using UV-Light Irradiation, on *S. Aureus* and *P. Aeruginosa*. *Mater. Today Proc.* **2019**, *18*, 920–927.
48. Masilan, K.; Neethiselvan, N.; Shakila, R.J.; Muralidharan, N.; Karthy, A.; Ravikumar, T.; Parthiban, F. Investigation on the coacervation of fish scale gelatin hydrogel with seafood waste hydrolysates for the development of artificial fish bait: Physico-chemical, thermodynamic, and morpho-structural properties. *J. Indian Chem. Soc.* **2022**, *99*, 100783.
49. Zhang, L.; Zheng, S.; Hu, Z.; Zhong, L.; Wang, Y.; Zhang, X.; Xue, J. Preparation of Polyvinyl Alcohol/Bacterial-Cellulose-Coated Biochar–Nanosilver Antibacterial Composite Membranes. *Appl. Sci.* **2020**, *10*, 752.
50. Thakur, K.; Kalia, S.; Kaith, B.; Pathania, D.; Kumar, A.; Thakur, P.; Knittel, C.E.; Schauer, C.L.; Totaro, G. The development of antibacterial and hydrophobic functionalities in natural fibers for fiber-reinforced composite materials. *J. Environ. Chem. Eng.* **2016**, *4*, 1743–1752.
51. Bugatti, V.; Zuppardi, F.; Viscusi, G.; Gorrasi, G. Active Packaging Based on Coupled Nylon/PE Pouches Filled with Active Nano-Hybrid: Effect on the Shelf Life of Fresh Milk. *Nanomaterials* **2021**, *11*, 1881.
52. Bahrami, A.; Mokarram, R.R.; Khiabani, M.S.; Ghanbarzadeh, B.; Salehi, R. Physico-mechanical and antimicrobial properties of tragacanth/hydroxypropyl methylcellulose/beeswax edible films reinforced with silver nanoparticles. *Int. J. Biol. Macromol.* **2019**, *129*, 1103–1112.
53. Radwan, E.K.; El-Naggar, M.E.; Abdel-Karim, A.; Wassel, A.R. Multifunctional 3D cationic starch/nanofibrillated cellulose/silver nanoparticles nanocomposite cryogel: Synthesis, adsorption, and antibacterial characteristics. *Int. J. Biol. Macromol.* **2021**, *189*, 420–431.
54. Chen, G.; He, L.; Zhang, P.; Zhang, J.; Mei, X.; Wang, D.; Zhang, Y.; Ren, X.; Chen, Z. Encapsulation of green tea polyphenol nanospheres in PVA/alginate hydrogel for promoting wound healing of diabetic rats by regulating PI3K/AKT pathway. *Mater. Sci. Eng. C* **2020**, *110*, 110686.
55. Khalaki, M.A.; Moameri, M.; Ghorbani, A.; Alagoz, S.M.; Dolatabadi, N.; Lajayer, B.A.; van Hullebusch, E.D. Chapter 8—Effects, uptake and translocation of Ag-based nanoparticles in plants. In *Toxicity of Nanoparticles in Plants*; Rajput, V.D., Minkina, T., Sushkova, S., Mandzhieva, S.S., Rensing, C., Eds.; Academic Press: Cambridge, MA, USA, 2022; pp. 171–192.
56. Jiang, B.; Tian, C.; Song, G.; Pan, Q.; Wang, Z.; Shi, L.; Qiao, Y.; Fu, H. A green route to synthesize novel Ag/C antibacterial agent, *Mater. Res. Bull.* **2012**, *47*, 458-463.

57. Vityazev, F.V.; Khramova, D.S.; Saveliev, N.Y.; Ipatova, E.A.; Burkov, A.A.; Beloserov, V.S.; Belyi, V.A.; Kononov, L.O.; Martinson, E.A.; Litvinets, S.G.; et al. Pectin–glycerol gel beads: Preparation, characterization and swelling behaviour. *Carbohydr. Polym.* **2020**, *238*, 116166.
58. Mathew, S.; Jayakumar, A.; Kumar, V.P.; Mathew, J.; Radhakrishnan, E.K. One-step synthesis of eco-friendly boiled rice starch blended polyvinyl alcohol bionanocomposite films decorated with in situ generated silver nanoparticles for food packaging purpose. *Int. J. Biol. Macromol.* **2019**, *139*, 475–485.
59. Li, Q.; Lu, F.; Zhou, G.; Yu, K.; Lu, B.; Xiao, Y.; Dai, F.; Wu, D.; Lan, G. Silver Inlaid with Gold Nanoparticle/Chitosan Wound Dressing Enhances Antibacterial Activity and Porosity, and Promotes Wound Healing. *Biomacromolecules* **2017**, *18*, 3766–3775.
60. Li, K.; Zhang, B.; Yang, Z.; Jiang, X.; Li, X. Degradation behaviors of silicone gel encapsulation material with moisture intrusion. *Polym. Degrad. Stab.* **2022**, *206*, 110197.
61. Aghaei, F.; Tangestaninejad, S.; Bahadori, M.; Moghadam, M.; Mirkhani, V.; Mohammadpoor−Baltork, I.; Khalaji, M.; Asadi, V. Green synthesize of nano-MOF-ethylcellulose composite fibers for efficient adsorption of Congo red from water. *J. Colloid Interface Sci.* **2023**, *648*, 78–89.
62. Chen, L.; Mi, B.; He, J.; Li, Y.; Zhou, Z.; Wu, F. Functionalized biochars with highly-efficient malachite green adsorption property produced from banana peels via microwave-assisted pyrolysis. *Bioresour. Technol.* **2023**, *376*, 128840.